# Formation mechanism of glycolaldehyde and ethylene glycol in astrophysical ices from HCO • and • CH 2 OH recombination: an experimental study

T. Butscher, Fabrice Duvernay, P. Theule, G. Danger, Yannick Carissan, Denis Hagebaum-Reignier, T. Chiavassa

Mon. Not. R. Astron. Soc. **000**, 1–?? (2015) Printed 22 July 2015 (MN LATEX style file v2.2)

# Formation mechanism of glycolaldehyde and ethylene glycol in astrophysical ices from $HCO^{\bullet}$ and $^{\bullet}CH_2OH$ recombination: an experimental study

T. Butscher[1], F. Duvernay[1⋆], P. Theule[1], G. Danger[1], Y. Carissan[2], D. Hagebaum-Reignier[2], T. Chiavassa[1]
[1] *PIIM, UMR 7345, Aix-Marseille Université, Avenue Escadrille Normandie-Niemen 13397 Marseille, France*
[2] *Aix Marseille Université, Centrale Marseille, CNRS, iSm2 UMR 7313, Marseille, 13397, France.*

Accepted . Received ; in

**ABSTRACT**
Among all existing complex organic molecules, glycolaldehyde $HOCH_2CHO$ and ethylene glycol $HOCH_2CH_2OH$ are two of the largest detected molecules in the interstellar medium. We investigate both experimentally and theoretically the low-temperature reaction pathways leading to glycolaldehyde and ethylene glycol in interstellar grains. Using infrared spectroscopy, mass spectroscopy and quantum calculations, we investigate formation pathways of glycolaldehyde and ethylene glycol based on $HCO^{\bullet}$ and $^{\bullet}CH_2OH$ radical-radical recombinations. We also show that $^{\bullet}CH_2OH$ is the main intermediate radical species in the $H_2CO$ to $CH_3OH$ hydrogenation processes. We then discuss astrophysical implications of the chemical pathway we propose on the observed gas-phase ethylene glycol and glycolaldehyde.

**Key words:** circumstellar matter – infrared: stars.

## 1 INTRODUCTION

Observations of the interstellar medium leads to the identification of approximately 180 molecules. Among them, more than 50 present six or more atoms (H, C, N or O): the so called complex organic molecules (COMs) (Woods et al. 2013). In star forming regions, these COMs are likely to be incorporated in the forming material of small bodies, such as comets, asteroids or planetesimals, and could have played a role in the emergence of life in the early Earth. Between all of these COMs, there is a particular interest in glycolaldehyde (GA) $HOCH_2CHO$ and in ethylene glycol (EG) $HOCH_2CH_2OH$.

First observed in Sagittarius B2 North Large Molecule Heimat (SB2N-LMH)(Hollis et al. 2000), glycolaldehyde (hereafter GA) has then been discovered in other systems, such as the hot molecular core G31.41+0.31 (Beltrán et al. 2009), IRAS 16293-2422 protostar (Jørgensen et al. 2012) or more recently NGC 1333-IRAS2A protostar (Coutens et al. 2015). Moreover, Hollis et al. (2001) showed that glycolaldehyde was present near the LMH source, but also in a less dense cloud extremities in the vicinity of the LMH core source with a larger spacial scale contrary to its isomers acetic acid $CH_3COOH$ and methylformate $CH_3OCHO$ that are concentrated in a small spacial scale nearby the source. Ethylene glycol (hereafter EG) was detected by Crovisier et al. (2004) in the comet C/1995 O1 (Hale-Bopp) but also in SB2N-LMH (Hollis et al. 2002) and NGC 1333-IRAS2A protostar (Maury et al. 2014) and is considered as one of the largest molecules identified in a comet by optical spectroscopy.

The purpose of this paper is to investigate the formation mechanisms of two molecules, GA and EG in astrophysical environments, which are not well understood. Several studies tried to explain their formation in such environment using two different pathways based on recombination of radicals. The first pathway is the recombination of hydroxymethyl radicals $^{\bullet}CH_2OH$ between them or with $HCO^{\bullet}$ to yield ethylene glycol and glycolaldehyde, respectively (Bennett & Kaiser 2007) :

$$\begin{aligned} {}^{\bullet}CH_2OH + HCO^{\bullet} &\longrightarrow HOCH_2CHO \\ {}^{\bullet}CH_2OH + {}^{\bullet}CH_2OH &\longrightarrow HOCH_2CH_2OH \end{aligned} \quad (1)$$

The second pathway is the $HCO^{\bullet}$ dimerisation leading to glyoxal and followed by successive hydrogenations (Fedoseev et al. 2015; Woods et al. 2013) to produce successively the two target molecules, GA and EG :

$$\begin{aligned} HCO^{\bullet} + HCO^{\bullet} &\longrightarrow HCOCHO \\ HCOCHO &\xrightarrow{+2H} HOCH_2CHO \\ HOCH_2CHO &\xrightarrow{+2H} HOCH_2CH_2OH \end{aligned} \quad (2)$$

⋆ E-mail:f.duvernay@univ-amu.fr (FD)

The formation of these radicals ($HCO^{\bullet}$ and $^{\bullet}CH_2OH$) may be initiated in cold regions of the MIS by CO hydrogenation processes occurring on interstellar grain-surface (Hama & Watanabe 2013):

$$CO \xrightarrow{+H} HCO^{\bullet} \xrightarrow{+H} H_2CO \xrightarrow{+H} \begin{cases} {}^{\bullet}CH_2OH \\ CH_3O^{\bullet} \end{cases}$$

$$\begin{cases} {}^{\bullet}CH_2OH \\ CH_3O^{\bullet} \end{cases} \xrightarrow{+H} CH_3OH$$

However, radicals are not easy to study in solid environment due to their high reactivity, even at low temperature. To make this study easier and to monitor the reaction processes, we use the cryogenic matrix-isolation technique. This method was used in several experiments to analyse $^{\bullet}CH_2OH$ from $CH_3OH$ photolysis (Jacox & Milligan 1973; Jacox 1981), or formyl radical $HCO^{\bullet}$ from hydrogenation of CO with non-energetic H-atoms (Pirim & Krim 2011). This way, we are able to trap radicals and isolate them from one another. Thus, since molecules are isolated from one another, infrared absorptions are close to those observed in gas-phase without rotational structure. Moreover, another advantage of the matrix-isolation technique is that it also increases stability and lifetime of radicals, due to the low-temperature environment allowing to probe them easily by infrared spectroscopy.

In this contribution, we photolyse $H_2CO$ in rare gas (hereafter Rg) matrices (Ar, Xe) at low temperature (12 K) to create radicals and "free" H-atoms inside the matrix. The annealing of our system will lead to the formation of new radicals species, especially $^{\bullet}CH_2OH$ from $H_2CO$ hydrogenation within the Rg matrices. *One has to keep in mind that rare gas matrices do not reproduce interstellar environment but enable isolation and characterization of radical species. With the disappearance of the rare gas by heating the sample, these unstable species are then freed and will react to create GA and EG by radical-radical recombination as it may occur in interstellar ices*

After a description of our experimental setup (Section 2), we describe results obtained from the three steps of our experiments (irradiation of $H_2CO$ in Ar and Xe matrices, annealing of the matrices and sublimation of rare gas) using mass and infrared spectrometries. To strengthen the characterization of intermediate species, DFT calculations were performed using B3LYP functional. Consequences on astrophysical detection of these molecules are given in the discussion part of this manuscript.

## 2 EXPERIMENTAL SETUP

### 2.1 Products

Argon and xenon (99.999 % of purity) used as matrix gases were purchased from Air Liquide. Formaldehyde was purchased as a polymer from Sigma Aldrich (99.95 % of purity) and was heated to about 90°C to produce the gas-phase monomer. Glycolaldehyde (hereafter denoted GA) was purchased as a dimer respectively from Sigma Aldrich (99.95 % of purity) and heated under vacuum to about 80°C to produce gas-phase monomer. Ethylene glycol (hereafter denoted EG) and methanol (99.95 % of purity) were purchased from Sigma Aldrich.

### 2.2 Experimental details

All experiments described are performed in a high vacuum chamber with a background pressure of $10^{-8}$ mbar at 295 K and $10^{-9}$ mbar at 12 K. Temperature is controlled using a model 21 CTI cold head, a resistive heater and a Lakeshore 331 temperature controller, in typical 4 K $min^{-1}$ temperature ramp.

Products were mixed in 2/1000 ratio of $H_2CO$/Rg in a Pyrex vacuum line using standard manometric techniques. The gaseous mixture was deposited at a rate of $5.10^{-2}$ mbar $s^{-1}$ (5 $\mu$mole $s^{-1}$) on a gold-plated surface kept at 30 K for xenon experiments and 12 K for argon experiments. Glycolaldehyde and ethylene glycol solid films can be obtained by directly dosing them onto the sample holder in order to get spectroscopic references.

Radicals are produced from VUV photolysis of formaldehyde $H_2CO$ in a rare gas matrix. The VUV photons are generated from a microwave induced $H_2$ plasma using a magnetic microwave magnetic applicator (Boreal Plasma) fed by a microwave generator (Opthos instruments). The $H_2$ plasma spectrum is dominated by Lyman alpha photons at 121.6 nm. The VUV flux is transmitted from the plasma chamber to the vacuum chamber through an $MgF_2$ window. Photon flux has been measured using the $O_2 \rightarrow O_3$ actinometry method (Cottin et al. 2003) to *c.a.* 2.5 $10^{13}$ photons.$cm^{-2}$.$s^{-1}$, which is $10^{10}$ times larger than the UV secondary flux in dense molecular clouds. In a typical experiment, radical-radical recombination products are obtained by desorbing the rare gas by warming the matrix until 35 K for experiments with Ar and until 85 K for experiments in Xe.

Infrared spectra of the different species were recorded in reflection-absorption mode between 4000 and 600 $cm^{-1}$ using a Bruker Tensor 27 FTIR spectrometer with MCT detector. Each spectrum was averaged over 20 scans with a 0.5 $cm^{-1}$ resolution, except for the background averaged over one hundred scans with the same resolution.

For quantification, the amount of GA is obtained from the band at 1111 $cm^{-1}$ ($\mathcal{A}$ = 8.1 $\times 10^{-18}$ cm $molecule^{-1}$) and the amount of EG is obtained from the bands at 1089 and 1047 $cm^{-1}$ (with a combined strength $\mathcal{A} = 7.8 \times 10^{-18}$ cm $molecule^{-1}$) (Hudson et al. 2005). Finally, the amount of methanol $CH_3OH$ is obtained from the band at 1023 $cm^{-1}$ with a band strength of $\mathcal{A} = 1.8 \times 10^{-17}$ cm $molecule^{-1}$ (Kerkhof et al. 1999).

Mass spectra were monitored using a RGA quadrupole mass spectrometer (MKS Microvision-IP plus) as the products desorb during the controlled temperature ramp. The ionization source was a 70 eV impact electronic source and the mass spectra were recorded between 1 and 100 amu in a full scan. After rare gas desorption, a ramp of 4 K $min^{-1}$ is applied while the ion current is recorded to obtain a full temperature programmed desorption (TPD) profile, relative to various products.

### 2.3 Computational methods

Density Functional Theory calculations were performed using the TURBOMOLE program package (Ahlrichs et al. 1989). The B3-LYP functional (Becke 1993) was used with the def2-TZVP basis set (Weigend & Ahlrichs 2005). The

resolution of identity approximation was used for every DFT calculations (Treutler & Ahlrichs 1995). Except if specified, all molecules were characterized as minima of the potential energy surface by computation of harmonic frequencies with the aoforce module (Deglmann et al. 2004). The zero point energy was added to the electronic energy. Harmonic frequencies were corrected by a scaling fact of 0.986 for B3LYP/def2-TZVP as optimized by Alecu et al. (2010). No symmetry was forced and input geometries were always built with no symmetry. One exception to this rule is the planar $HCO^{\bullet}$ molecule treated in the $C_s$ point group of symmetry.

## 3 RESULTS

### 3.1 VUV photolysis of $H_2CO$ in Ar and Xe matrices at 12 K: formation of the $HCO^{\bullet}$ radical

We first *perform* the VUV photolysis of $H_2CO$ at Lyman-$\alpha$ in solid Rg in order to form the $HCO^{\bullet}$ radicals. Figure 1 displays the difference infrared spectra showing the evolution of the $H_2CO$/Rg photolysis experiments.

Infrared spectrum of monomeric $H_2CO$ isolated in solid Xe is displayed in Fig. 1 as negative bands whereas all the newly formed products appear as positive bands. The fundamental observed bands of $H_2CO$ ($^{12}C$ and $^{13}C$) in both Xe and Ar matrices are listed in Table 1. In Xe experiment, the infrared spectrum of $H_2CO$ is dominated by the strong absorptions at 2837, 2778, 1735, and 1491 $cm^{-1}$ assigned to the asymmetric CH stretching mode, symmetric CH stretching mode, C=O stretching mode, and CH bending mode, respectively. These bands are down-shifted at 2822, 2767, 1697, and 1491 $cm^{-1}$ in the case of $H_2^{13}CO$ isotopologue (Table 1). The corresponding values in Ar matrix are listed in Table 1.

These spectra are in good agreement with previous studies and shows that $H_2CO$ is mainly isolated as a monomer (Nelander 1980a,b).

**Table 1.** Infrared absorption bands and assignment of $H_2CO$ in rare gas matrix at 12 K.

| Wavenumbers ($cm^{-1}$) | | | | |
|---|---|---|---|---|
| $^{12}C$ | | $\Delta\nu(^{12}C - ^{13}C)$ | | |
| Ar | Xe | Ar | Xe | Assignments |
| 3464 | 3449 | 75 | 74 | $2\nu$(CO) |
| 2997 | 2981 | 43 | 37 | $2\delta$(CH) |
| 2864 | 2837 | 18 | 15 | $\nu$(CH) - a |
| 2798 | 2778 | 5 | 11 | $\nu$(CH) - s |
| 2719 | 2700 | 11 | 9 | - |
| 1742 | 1735 | 38 | 38 | $\nu$(CO) |
| 1499 | 1491 | 0 | 0 | $\delta$(CH) |
| 1245 | 1238 | 10 | 8 | $\rho$(CH) |
| 1168 | 1163 | 12 | 12 | $\omega$(CH) |

$\nu$: stretching; $\delta$: bending; $\rho$: rocking; $\omega$: wagging

Table 2 summarizes the band positions of the products identified after the VUV photolysis at 12 K in Ar and Xe matrices for the formaldehyde and its $^{13}C$ isotopologue. After VUV irradiation in Xe matrix, the formation of monomeric CO is observed through its strong band located at 2133 $cm^{-1}$. Beside the CO formation, we clearly observe the formyl radical ($HCO^{\bullet}$) from its infrared absorption located at 2442, 1857 and 1082 $cm^{-1}$ assigned to the CH stretching mode, C=O stretching mode, and CH bending mode respectively (Fig.1, Table 2). These absorptions are observed in Ar matrix at 2482, 1864, 1086 $cm^{-1}$ in accordance with literature values reported by Milligan & Jacox (1969).

The calculated harmonic vibrational frequencies for this species are quite close to the experimental ones (Fig. 1, Table 2). The calculated shifts from $^{12}C$ to $^{13}C$ are also very well reproduced. The largest discrepancy is observed for the CH stretching mode of $HCO^{\bullet}$. This is due to a strong anharmonicity in this mode as extensively reported in the literature (Werner et al. 1995; Serrano-Andrés et al. 1998; Keçeli et al. 2009).

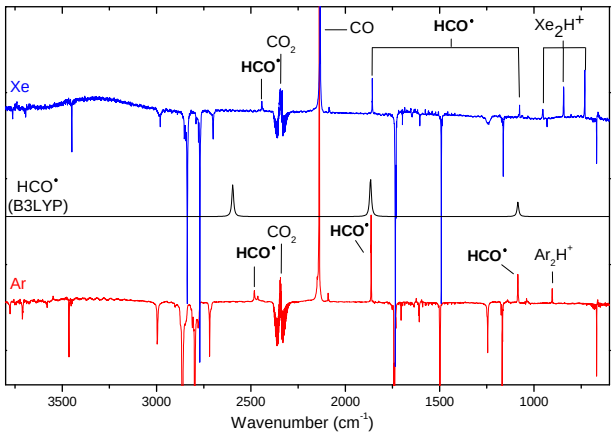


**Figure 1.** Difference infrared spectra representing the evolution of CO, $HCO^{\bullet}$, $Rg_2H^+$ species at 12 K after 22 h VUV irradiation of $H_2CO$/Rg (2/1000) compared to the reference spectrum recorded at 12 K before irradiation. Experimental spectra are compared with the calculated infrared spectrum of $HCO^{\bullet}$ radical at the B3LYP/def2-TZVP level of theory. Infrared absorption bands associated with formed species after photolysis appear as positive bands, those of formaldehyde as negative bands.

Infrared absorptions are also observed at 953, 843, and 731 $cm^{-1}$ in Xe matrix assigned to $Xe_2H^+$ or in Ar matrix at 903 $cm^{-1}$ assigned to $Ar_2H^+$, attesting the formation of "free" H-atoms during photolysis (Kunttu et al. 1992). Indeed, it has been extensively reported that UV photolysis of small hydrides in solid Rgs forms ionic species $RgHRg^+$ (Rg=Ar, Kr, and Xe) (Pettersson et al. 2000).

The UV photolysis using mercury arc lamp ($\lambda > 250$ nm) of formaldehyde in Ar matrix at 12 K has been previously investigated (Sodeau & Lee 1978; Diem & Lee 1979). They report formation of isolated CO, whereas no evidence of formyl radical production is observed at such wavelength. They also observe formation of glycolaldehyde ($HOCH_2CHO$) but only in concentrated $H_2CO$/Ar matrix (1/40) (Sodeau & Lee 1978). They suggest that the dimer of formaldehyde could be at the origin of the glycolaldehyde formation. In our conditions, no evidence of glycolaldehyde at 12 K after irradiation of $H_2CO$/Rg is observed, confirming that $H_2CO$ is mainly isolated as a monomer.

**Table 2.** Infrared absorption and assignments of observed bands after VUV irradiation (22 h) at 12 K and after annealing (35 K for Ar experiment, 50 K for Xe experiment).

| After irradiation | | | | After annealing | | | | | | | |
|---|---|---|---|---|---|---|---|---|---|---|---|
| Wavenumbers ($cm^{-1}$) | | | | Wavenumbers ($cm^{-1}$) | | | | | | | |
| $^{12}C$ | | $\Delta\nu(^{12}C$ -$^{13}C)$ | | $^{12}C$ | | $\Delta\nu(^{12}C$ -$^{13}C)$ | | Theory[a] | | | |
| Ar | Xe | Ar | Xe | Ar | Xe | Ar | Xe | $^{12}C$ | $\Delta\nu(^{12}C$ -$^{13}C)$ | Assignments | Molecules |
| 2482 | 2442 | 6 | 6 | 2482 | 2442 | 6 | 6 | 2604 | 7 | $\nu$(CH) | **HCO$^\bullet$** |
| 2344 | 2334 | 65 | 65 | 2344 | 2334 | 65 | 65 | - | - | $\nu$(CO) | $CO_2$ |
| 2138 | 2133 | 47 | 47 | 2138 | 2133 | 45 | 47 | - | - | $\nu$(CO) | CO |
| - | - | - | - | 2137 | 2132 | 48 | 47 | - | - | $\nu$(CO) | CO dimer |
| 1864 | 1857 | 40 | 40 | 1864/1851 | 1857 | 40 | 39 | 1907 | 41 | $\nu$(CO) | **HCO$^\bullet$** |
| - | - | - | - | 1843 | - | 31 | - | 1874 | 44 | $\nu$(C=O) | **HOCO$^\bullet$** |
| - | - | - | - | 1358 | 1355 | - | 5 | 1339 | 7 | $\delta$(HOC) | **$^\bullet$CH$_2$OH** |
| - | - | - | - | 1211 | - | - | - | 1219 | 3 | $\delta$(HOC) | **HOCO$^\bullet$** |
| - | - | - | - | 1196 | - | - | - | - | - | - | * |
| - | - | - | - | 1188 | - | - | - | - | - | $\delta$(CH) | **$^\bullet$CH$_2$OH:CO** |
| - | - | - | - | - | 1180 | - | 0 | - | - | - | $XeH_2$ |
| - | - | - | - | 1183 | 1176 | 15 | 14 | 1185 | 20 | $\delta$(CH) | **$^\bullet$CH$_2$OH** |
| - | - | - | - | - | 1166 | - | 0 | - | - | - | $XeH_2$ |
| - | - | - | - | 1117 | - | - | - | - | - | - | * |
| 1086 | 1082 | 8 | 6 | 1086/1085 | 1082 | 8 | 6 | 1092 | 7 | $\delta$(CHO) | **HCO$^\bullet$** |
| - | - | - | - | 1065 | 1059 | - | 17 | 1067 | 19 | $\nu$(C-O) | **HOCO$^\bullet$** |
| - | - | - | - | 1048 | 1044 | - | 4 | 1041 | 2 | $\delta$(HCOH) | **$^\bullet$CH$_2$OH** |
| - | - | - | - | 1039 | 1027 | 16 | 16 | - | - | $\nu$(C-O) | $CH_3OH$:CO |
| - | - | - | - | 1034 | 1025 | 16 | 15 | - | - | $\nu$(C-O) | $CH_3OH$ |
| - | 953 | - | 0 | - | - | - | - | - | - | - | $Xe_2H^+$ |
| 903 | - | 0 | - | - | - | - | - | - | - | - | $Ar_2H^+$ |
| - | 843 | - | 0 | - | - | - | - | - | - | - | $Xe_2H^+$ |
| - | 731 | - | 0 | - | - | - | - | - | - | - | $Xe_2H^+$ |
| - | - | - | - | 706 | 700 | - | 0 | 700 | 6 | $\gamma$(HCOH) | **CH$_3$O$^\bullet$**[b] |

$\nu$: stretching; $\delta$: bending; $\gamma$: rocking.
[a]: B3LYP - def2-TZVP basis set. [b]: tentatively

### 3.2 Reaction of mobile hydrogen atoms: formation of the $^{\bullet}CH_2OH$ radicals

When annealing the photolyzed Rg matrices, trapped H-atoms can diffuse and hydrogenate unsaturated species formed by the previous irradiation (CO, $HCO^{\bullet}$, and $H_2CO$)(Pettersson et al. 1999). It has been shown that global diffusion of H-atoms starts at about 40 K and 30 K in Xe and Ar matrices respectively. (Pettersson et al. 1999, 2000; Khriachtchev et al. 2002). The photolysed $H_2CO$/Rg matrices have been warmed at 50 K in Xe and at 30 K in Ar for 5 min and then cooled down to 12 K (first annealing cycle).

Figure 2 displays the difference infrared spectra showing the effect of annealing of the photolysed $H_2CO$/Rg matrices. Clearly hydrogenation processing occurs at this temperature. Indeed, the amount of $HCO^{\bullet}$ radicals increases (positive bands) whereas the band of CO decreases (negative band) as seen in the difference spectra (Fig. 2). We observe the decrease of bands associated to $Rg_2H^+$ (953, 843, and 731 $cm^{-1}$ in Xe experiment and 903 $cm^{-1}$ in Ar experiment) due to the neutralisation of this species during annealing which may also release "free" H-atoms within the matrix (Fig. 2, Table 2). At the same time, in Xe experiment, two strong bands at 1180 and 1166 $cm^{-1}$ are also observed and are assigned to the $XeH_2$ species (Khriachtchev et al. 2002; Pettersson et al. 2000). This phenomenon has been intensively studied and it is the result of the migration of H-atoms during the warming (Khriachtchev et al. 2002; Pettersson et al. 2000). It has to be noted that the species $ArH_2$ is not observed in Ar matrix.

Hydrogenation of $H_2CO$ can lead to the formation of two radical species $^{\bullet}CH_2OH$ and $CH_3O^{\bullet}$. Figure 3 displays the difference infrared spectra showing the effect of annealing in both Ar and Xe matrices in the characteristic zone of $^{\bullet}CH_2OH$ and $CH_3O^{\bullet}$ radicals. In Ar matrix, we clearly observe formation of the $^{\bullet}CH_2OH$ through its absorption bands located at 1358, 1183, and 1048 $cm^{-1}$ in good agreement with the values reported in solid Ar (Jacox & Milligan 1973; Jacox 1981). The band located at 1188 $cm^{-1}$ is tentatively assigned to the $^{\bullet}CH_2OH$:CO complex due to the diffusion of CO during annealing (Duvernay et al. 2004; Dubost & Abouaf-Marguin 1972). This hypothesis is also supported by the formation during annealing of the CO dimer at 2137 $cm^{-1}$ (Dubost & Abouaf-Marguin 1972) (Fig. 3, Table 2). The formation of the $^{\bullet}CH_2OH$ radical is also observed after annealing in solid Xe through its bands located at 1355, 1176 and 1044 $cm^{-1}$ (Fig. 3, Table 2). The absorption band positions of $^{13\bullet}CH_2OH$ in both solid Xe and Ar are summarized in Table 2. Again these values are in good agreement with the values reported by Jacox (1981) in solid Ar. The calculated harmonic vibrational frequencies of $^{\bullet}CH_2OH$, as well as the calculated frequency shifts $\Delta\nu(^{12}C - ^{13}C)$ are quite close to the experimental ones (Fig. 3, Table 2) which strengthen our previous assignments.

Due to the lack of vibrational data on the $CH_3O^{\bullet}$ radical, DFT calculations were performed on this species. The corresponding calculated spectrum is displayed in Fig. 3. The most intense calculated infrared band of $CH_3O^{\bullet}$ is located at 700 $cm^{-1}$. Accordingly, we tentatively assigned a small band at 700 $cm^{-1}$ in Xe experiment and at 706 $cm^{-1}$ in Ar experiment to the $CH_3O^{\bullet}$ radical. In $^{13}C$ experiments, the corresponding bands are also present and are listed in Table 2. Since we only observed in both Ar and Xe experiments the most intense band of this compound, it may indicate this radical is produced in very small quantity as compared to $^{\bullet}CH_2OH$. Moreover, we also observe that the quantity of $CH_3O^{\bullet}$ is more important in Xe experiments than in Ar experiments. It can be explained by the difference of photolysis rates. The effective photolysis rate is far greater in Ar environment, leading to a smaller quantity of $H_2CO$ in this system after irradiation than in Xe matrix. Thus, assuming that $CH_3O^{\bullet}$ is produced from $H_2CO$ hydrogenation, a smaller quantity of $CH_3O^{\bullet}$ would be formed in Ar matrix than in Xe matrix.

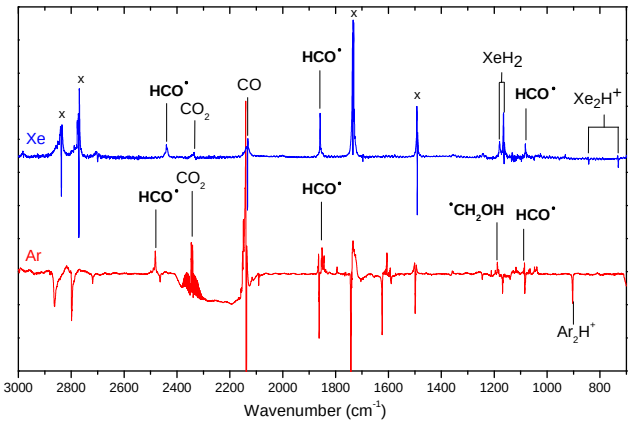


**Figure 2.** Difference infrared spectra showing the effect of annealing (30 K in Ar and 50 K in Xe) compared with the infrared spectra recorded at 12 K after 22 h of VUV irradiation. All the bands labeled with a cross are $H_2CO$ absorption bands. Infrared absorption bands associated with formed species during annealing appear as positive bands, those of consumed species as negative bands.

Finally, the last hydrogenated product observed after the annealing is the fully saturated CO bearing molecule, the methanol $CH_3OH$ coming from the hydrogenation of the $^{\bullet}CH_2OH$ and/or $CH_3O^{\bullet}$ radicals (Fig. 3, Table 2). It has to be noted that we also observed the formation of $CH_3OH$: CO complex at 1039 $cm^{-1}$ (Diem & Lee 1979) during the annealing due to CO diffusion as already mentioned. Other products are also formed during the annealing such as $CO_2$ or $HOCO^{\bullet}$ radical (Table 2). **Thus after annealing of the photolysed $H_2CO$/Rg matrix in our experimental conditions, the radical species observed are the $HCO^{\bullet}$, $^{\bullet}CH_2OH$, traces of $HOCO^{\bullet}$, and possibly $CH_3O^{\bullet}$.** Two supplementary cycles of annealing have been performed during 10 and 15 min respectively without increasing the amount of hydrogenated products meaning that all "free" H-atoms trapped within the matrices have already reacted during the first annealing. In the next section, we will investigate the reactivity of the main formed radicals, namely $HCO^{\bullet}$ and $^{\bullet}CH_2OH$ by sublimating the Rg matrices. Indeed the observed radicals are isolated from one another by the Rg atoms and thus cannot recombine. By removing the Rg matrix, the radicals will be free to recombine forming new species.

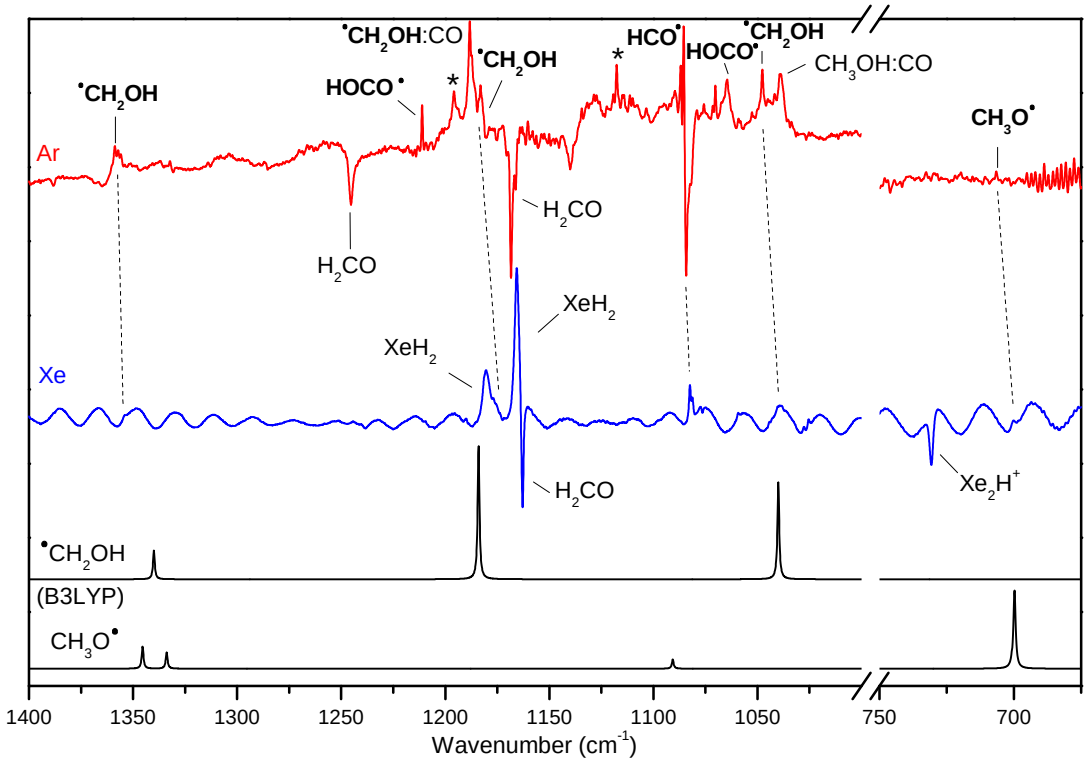


**Figure 3.** Difference infrared spectra showing the effect of annealing (50 K in solid Xe and 30 K in solid Ar). The reference spectrum used for the difference is the infrared spectrum recorded at 12 K after 22 h of VUV irradiation before annealing. Infrared absorption bands associated with formed species during annealing appear as positive bands, those of consumed species as negative bands. Experimental spectra are compared with the calculated infrared spectra of $^{\bullet}CH_2OH$ and $CH_3O^{\bullet}$ at the B3LYP/def2-TZVP level of theory. The stars label unknown species.

### 3.3 Matrix sublimation: radical recombination

The photolysed $H_2CO$/Rg matrices are then warmed at a rate of 4 K $min^{-1}$ until full sublimation of Rg that occurs at 35 K for solid Ar and 85 K for Solid Xe. After this process is completed, a solid film is obtained as shown in Fig. 4.

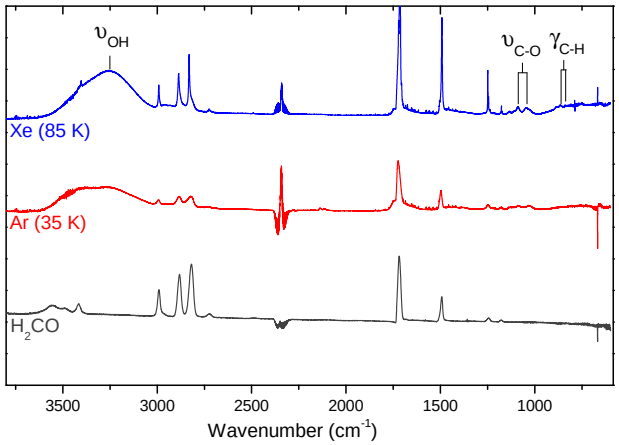


**Figure 4.** Infrared spectra of solid film obtained after sublimation of the photolysed Rg matrix at 12 K during 22 h. The infrared spectra are recorded at 85 K for Xe experiment and 35 K for Ar experiment. They are both compared with solid film of $H_2CO$ at 20 K.

Beside the infrared bands due to the remaining formaldehyde, CO, and $CO_2$ products already detected in Rg matrix, new bands are observed in both experiments in the OH, C=O, and C-O stretching mode regions, indicating that a reactivity occurs from radical recombination during the matrix sublimation. The same infrared absorption bands are observed in both Ar and Xe experiments suggesting that the Rg nature does not influence radical recombination. Table 3 summarizes the band positions of the products identified in the solid film of the Rg matrix sublimation of the $H_2CO$ photolysed during 22h for both $^{12}C$ and $^{13}C$ experiments.

To make the attribution of the new formed species easier, we warmed the sample up to 150 K (top spectrum in Fig.5) in order to remove the remaining formaldehyde. *It has to be noted that during the warming no reactivity occurs since no changes on IR spectra are observed. It indicates that all the radicals already reacted during the Rg sublimation.* Considering the new species formed from radical recombination occurring after Rg sublimation, glycolaldehyde (GA, $HOCH_2CHO$) was identified by its C=O stretching mode at 1745 $cm^{-1}$ (Bennett & Kaiser 2007; Hudson et al. 2005). We were also able to detect the CH rocking mode at 1374 $cm^{-1}$, and the CH twisting mode at 1232 $cm^{-1}$ (Fig.5)

The infrared spectrum of pure GA is displayed in Fig. 5 as reference and can be directly compared with the solid film obtained after photolysis and matrix sublimation (top spectrum). EG is detected through its bands located at 1089

**Table 3.** Infrared absorption band positions and vibrational mode assignments of new products formed after matrix desorption and radical recombination.

| Wavenumbers ($cm^{-1}$) | | | |
|---|---|---|---|
| $^{12}C$ | $\Delta\nu(^{12}C$ -$^{13}C)$ | Assignments | Molecule |
| 3238 | -16 | $\nu$(OH) | EG / GA |
| 2949 | 14 | $\nu$(CH) | EG |
| 2878 | 12 | $\nu$(CH) | EG |
| 1745 | 42 | $\nu$(C=O) | GA |
| 1707 | 37 | $\nu$(C=O) | Glyoxal[a] |
| 1699 | 35 | $\nu$(C=O) | GA |
| 1699 | 35 | - | EG |
| 1457 | 5 | $\delta$(CH) | EG / $CH_3OH$ |
| 1423 | 8 | $\delta$(OH) | EG / GA |
| 1407 | 2 | $\delta$(OH) | $CH_3OH$ |
| 1374 | 1 | $\delta$(CH) | GA |
| 1265 | 3 | $CH_2$ twist | EG |
| 1232 | 2 | $CH_2$ twist | GA |
| 1214 | 10 | $CH_2$ twist | EG |
| 1137 | 21 | - | * |
| 1111 | 22 | $\nu$(C-O) | GA |
| 1089 | 26 | $\nu$(C-O) | EG |
| 1047 | 23 | $\nu$(C-O) | EG / GA |
| 1023 | 31 | $\nu$(C-O) | $CH_3OH$ |
| 884 | 6 | $\gamma$(CH) | EG / GA |
| 865 | 16 | $\gamma$(CH) | EG |
| 857 | 16 | $\nu$(C-C) | GA |
| 755 | 19 | $\delta$(O=CC) | GA |

$\nu$: stretching; $\delta$: bending; $\rho$: rocking; $\gamma$: out of plane bending.
[a]: tentative

and 1047 $cm^{-1}$ assigned to the C-O stretching mode (Hudson et al. 2005). Again the pure spectrum of EG is displayed in Fig. 5 for direct comparison. The last product that can be securely identified from infrared spectroscopy is methanol from its bands at 1023 $cm^{-1}$ close to the C-O stretching mode of EG (Fig. 5). One has to keep in mind that contrary to GA and EG, methanol was already observed after annealing of the photolysed Rg matrix (section 3.2). The infrared spectrum of the solid film obtained after sublimation of the Rg matrix is compared in Fig. 5 with the summation spectrum of GA + EG + methanol (dashed line spectrum). The two spectra fit nicely, confirming the previous assignments. In addition, using the band strengths of methanol, GA, and EG given in the literature (see experimental section) we calculate the column density of products: $N$(methanol)= $3.9\times10^{15}$mol $cm^{-2}$, $N$(GA)= $3.3\times10^{15}$ mol $cm^{-2}$ and $N$(EG)= $1.7\times10^{16}$ mol $cm^{-2}$ giving a ratio of $N$(EG)/$N$(GA) of 5.1 in our conditions.

Only two bands cannot be reproduced in the summation spectrum at 1707 and 1137 $cm^{-1}$ that can be assigned to a C=O and C-O stretching modes respectively. We tentatively assigned the band located at 1707 $cm^{-1}$ to the C=O stretching mode of glyoxal CHOCHO (Verderame et al. 1970).

The assignment of the products observed in the solid film has been also confirmed by mass spectrometry. The

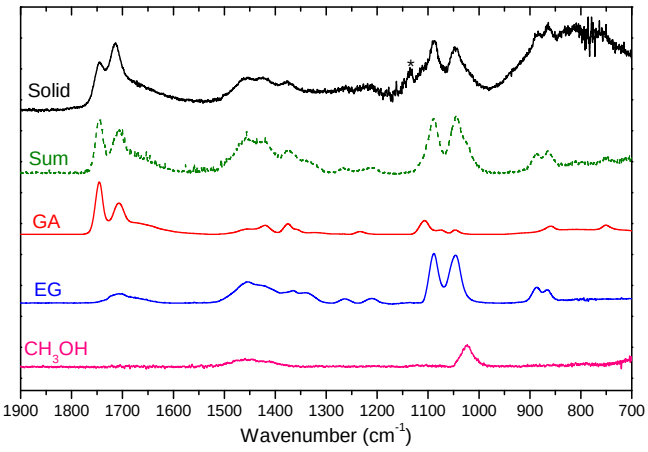


**Figure 5.** Infrared spectrum of the solid film obtained after sublimation of the photolysed $H_2CO$/Rg matrix at 12 K during 22 h recorded at 150 K (after sublimation of Rg and $H_2CO$). This spectrum is compared with pure ethylene glycol (EG), glycolaldehyde (GA), and methanol. The green spectrum (dashed line) is the summation of the reference spectra: Sum = EG + GA + methanol. Unknown species is labeled by a star (1137 $cm^{-1}$). The broad band observed near 800 $cm^{-1}$ is relative to OH libration mode of water.

newly formed species are monitored *in situ* by a temperature programmed desorption (TPD) using quadrupole mass spectrometry (QMS) to monitor in gas phase the thermally desorbed species. Figure 6 presents a typical QMS TPD spectra of the solid film obtained after sublimation of the Rg in the photolysed matrix. One can see that in the temperature range from 100- 300 K, five different products appears at 130, 147, 164, 195, and 214 K that are labeled (a), (b), (c), (d), and (e) in Fig. 6 respectively.

TPD QMS spectra provide information to identify the origin of the carriers. Indeed, molecules desorb at specific temperatures and fragmentation patterns upon electron impact induced dissociative ionization are characteristic of a molecular structure (right insets in Fig. 6).

Three products can be securely identified by comparing desorption temperature as well as the fragmentation patterns with values reported coming from our own references: (b)=$CH_3OH$ ($T_{des}$= 147 K; M=32), (d)=$HOCH_2CHO$ ($T_{des}$= 195 K; M=60), and (e)=$HOCH_2CH_2OH$ ($T_{des}$= 214 K; M=62). Indeed, the desorption temperature of the species (b) and (e) are consistent with those of references of methanol and EG respectively, as shown on the bottom part of the left insets in Fig. 6. A slight difference is observed for (d) species between experiment and GA reference. It can be explained by a mixture effect as previously shown by (Maity et al. 2015). In addition, fragmentation patterns of the desorbed species (b), (d), and (e) agree well with the reference mass spectra as shown in the right inset in Fig. 6. The small inconstancy in fragment intensities between reference spectra and desorbing species spectra are likely due to partial co-sublimation (Fedoseev et al. 2015; Maity et al. 2015). The products identification has been also confirmed by isotopic experiments with $^{13}C$ (see supplementary materials).

The species (a) that desorbs at 130 K is characterised by a $m/z$ 58 that shifts to $m/z$ 60 in the case of $^{13}C$ experiments. Thus, this species can be assigned to the molec-

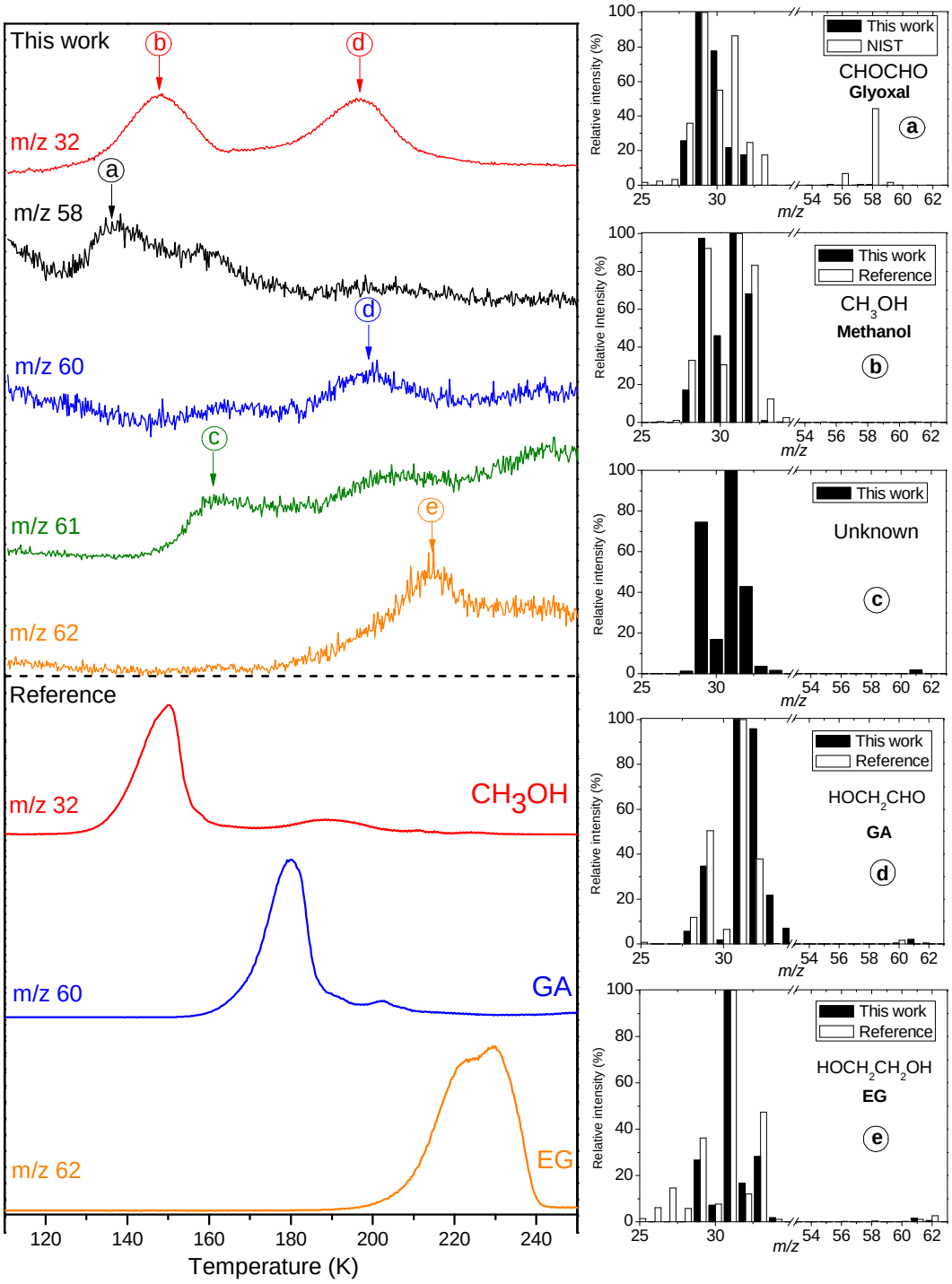


**Figure 6.** TPD spectra (4 K $min^{-1}$) of the solid film obtained after rare gas desorption of the photolysed $H_2CO$/Rg experiment. They are compared with TPD spectra of methanol ($m/z$ 32 : $CH_3OH^{+\bullet}$), glyoxal ($m/z$ 58 : $HCOCHO^{+\bullet}$), GA ($m/z$ 60 : $HOCH_2CHO^{+\bullet}$) and EG ($m/z$ 62 : $HOCH_2CH_2OH^{+\bullet}$) references. On the right hand of the figure compare the fragmentation patterns of desorbing species detected in this experiment upon 70 eV electron impact with references recorded in our laboratory. Detected species are indicated by a-e letters at their desorption temperature.

ular formula $C_2H_2O_2$. The most stable isomer with this molecular formula is the glyoxal HCOHCO, product already suspected to be formed from the infrared spectra analysis. However the reported desorption temperature of this compound in methanol matrix is 145 K (Maity et al. 2015). As previously mentioned, the differences observed between the desorption temperatures may be explained by partial co-sublimation with remaining formaldehyde that occurs around 110-120 K in our experimental conditions and also with methanol that occurs between 135 and 160 K. We also compared the fragmentation pattern of the desorbed species (a) at 130 K with mass spectrum of glyoxal taken

from NIST database (http://webbook.nist.gov/chemistry). The fragmentation patterns are quite different even if all fragments observed in the reference are present in our sample. Indeed they do not share the same intensity ratios, especially the ($m/z$ 28)/($m/z$ 58), ($m/z$ 29)/($m/z$ 58), and ($m/z$ 30)/($m/z$ 58) ratios. These ratios are higher in our sample than in the glyoxal reference. This is also consistent with co-sublimation with remaining formaldehyde and with methanol. Indeed the fragmentation patterns of these two species are dominated by $m/z$ 28, 29, and 30. Thus the observed fragmentation pattern observed at 130 K in our sample could be the sum of formaldehyde, methanol and glyoxal fragmentation patterns. However due to the incertitude previously mentioned, detection of glyoxal is not clear enough and accordingly will only be tentative. In any case, if it is formed, it is in such a low amount that prevents its clear identification.

Concerning the species (c) that desorbs at 164 K, we were unable to find any reference spectra matching with the fragmentation pattern. This species is characterised by several signals at $m/z$ 61, 60, 46, 45, 32, 31, 30, and 29 (Fig. 6). The higher mass detected for this species at $m/z$ 61 is an odd number. One has to keep in mind that because our starting material ($H_2CO$) is nitrogen-free, it indicates that $m/z$ 61 refers to a fragment of a larger molecule (according to the nitrogen rule of mass spectrometry). The identification of this compound is still under investigation and additional experiments will be performed soon.

**Finally, TPD QMS analysis confirms IR identification of the products observed after sublimation of the Rg matrix, namely methanol, glycolaldehyde, ethyleneglycol and possibly glyoxal**.

## 4 DISCUSSION : GA AND EG FORMATION FROM RADICAL RECOMBINATION

In this contribution, we used the Rg isolation matrix technique as a powerful method to study radical properties and reactivity. We photolyse $H_2CO$ in Ar and Xe matrices at low temperature (12 K) in order to control $HCO^\bullet$ and "free" H-atoms formation within the matrix. Subsequent annealing of our photolysed samples led to the formation of new radicals species from hydrogenation processes such as the $^\bullet CH_2OH$ radical. To our knowledge, this is the first experimental evidence showing that in the $H_2CO$ to $CH_3OH$ hydrogenation process, $^\bullet CH_2OH$ radical is an intermediate. However $CH_3O^\bullet$ radical has been already detected as an intermediate but only when H and CO are co-deposited rather than a direct H bombardment of CO ice (Pirim & Krim 2011; Fuchs et al. 2009).

Interestingly, the calculated barrier for the formation of $^\bullet CH_2OH$ and $CH_3O^\bullet$ from $H_2CO$ hydrogenation are 33 and 10 kJ mol$^{-1}$, respectively, that should prevent their formation at low temperature (Rimola et al. 2014). Tunnelling effects which can play a significant role at very low temperatures is often proposed as an explanation of the great discrepancy between the results obtained by laboratory experiments and the calculated energy barriers of hydrogenation reactions (Rimola et al. 2014; Fedoseev et al. 2015). Moreover, the way we form radicals (photodissociation followed by the Rg matrix sublimation) prevents electronically excited radicals to react.

We also demonstrate that radical recombination of $HCO^\bullet$ and $^\bullet CH_2OH$, previously generated in Rg matrices, forms GA, EG, and possibly glyoxal as soon as the sublimation of the Rg matrix is achieved. Indeed the formed radicals in Rg matrix are isolated from one another and thus cannot react in such isolated conditions. However as soon as the Rg is removed, they are no longer isolated and they are free to react as it follows:

$$HCO^\bullet + CH_2OH^\bullet \longrightarrow HOCH_2CHO$$
$$CH_2OH^\bullet + CH_2OH^\bullet \longrightarrow HOCH_2CH_2OH$$
$$HCO^\bullet + HCO^\bullet \longrightarrow HCOCHO \text{ (tentatively detected)}$$

*These reactions occur at 35 K in Ar and at 85 K in Xe, implying that temperature is not the dominant factor for the formation of GA and EG and may occur at lower temperature. The only need is the presence of the radicals before the matrix sublimation.*

One can think that $HCO^\bullet$ would also dimerise as easily as $^\bullet CH_2OH$ forming the glyoxal which is not the case since glyoxal is barely detected in our experiments probably due to its low quantity compared to the main product EG formed from the $^\bullet CH_2OH$ radical dimerisation.

This result may suggest that, in our experimental conditions, $HCO^\bullet$ is not as much reactive as the $^\bullet CH_2OH$ radical in solid state. Another explanation could come from $HCO^\bullet$ dimerisation mechanism observed in gas phase (Clark et al. 1978). It has been shown that $HCO^\bullet$ dimerisation in gas phase is dominated by:

$$2\,HCO^\bullet \longrightarrow H_2CO + CO$$

The same mechanism could also occur in solid phase, but in our experimental conditions, since CO and $H_2CO$ are initially present in solid film after Rg sublimation, we cannot confirm this hypothesis. Nevertheless, these experimental results suggest that glyoxal formation is unfavoured over GA and EG formation from $HCO^\bullet$ and $^\bullet CH_2OH$ radicals reactivity.

## 5 ASTROPHYSICAL IMPLICATIONS

Several authors have suggested possible GA and EG formation pathways under astrophysical conditions from theoretical (Woods et al. 2012, 2013) or experimental studies (Bennett & Kaiser 2007; Fedoseev et al. 2015). According to these studies, two different pathways seem to be likely to occur on the interstellar grains. The first one (mechanism (1) in Fig. 7)- supported by our works - involves the radical recombination of $HCO^\bullet$ with $^\bullet CH_2OH$ to form GA, and the radical $^\bullet CH_2OH$ dimerisation to form EG (Bennett & Kaiser 2007). The second one (mechanism (2) in Fig. 7) involves dimerisation of formyl radical ($HCO^\bullet$) leading to the formation of glyoxal followed by hydrogenation to form GA and EG (Fedoseev et al. 2015; Woods et al. 2013).

According to our experimental results, we show that GA and EG can be efficiently formed from $HCO^\bullet$ and $^\bullet CH_2OH$ radical reactivity at low temperature. We also show that glyoxal formation from $HCO^\bullet$ radical dimerisation is unfavoured over the GA and EG formation. This means that

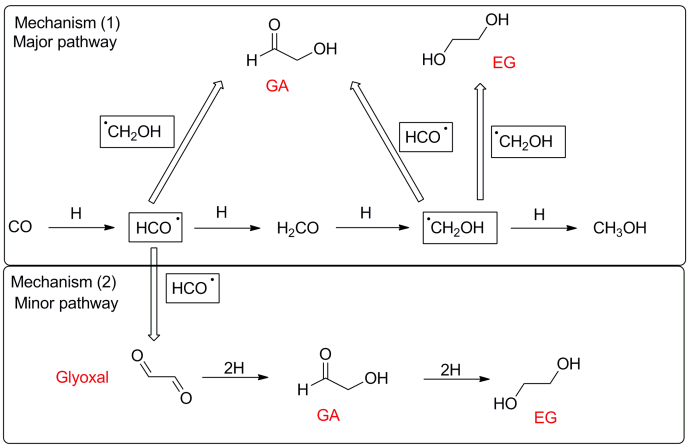


**Figure 7.** Scheme of GA and EG formation on interstellar grains.

mechanism (1) would be favoured over mechanism (2) as soon as both $HCO^{\bullet}$ and $^{\bullet}CH_2OH$ radicals are presents.

*In water-dominated interstellar ices, the molecule formation from radical-radical recombination implies mobility of unstable species. But, this mobility requires an increase of the local temperature that may prevent hydrogenation reactions. For example, dimerisation of $HCO^{\bullet}$ (mechanism (2)) would imply mobility of the radical species to form glyoxal. However, subsequent hydrogenation reactions would not be possible due to the higher local temperature. This means that, in such conditions, only glyoxal would be formed but not GA and EG. One can think that dimerisation of formyl radical could occur without mobility in case of hydrogenation reaction on pure CO ices. Indeed, both dimerisation and hydrogenation would be possible at temperature lower than 10 K, forming successively glyoxal, GA, and EG. This scenario would only be possible in cold regions of the ISM where hydrogenation reactions dominate.*

*In a same way, $HCO^{\bullet}$ and $^{\bullet}CH_2OH$ radicals can also be formed in cold molecular clouds from hydrogenation reactions on CO ices and then react to form GA and EG (mechanism (1)). Since this mechanism is based on one-step competitive reactions, GA and EG would be formed even if the local temperature is increasing. Indeed, in warmer region, the formation reaction rates can be significantly increased due to the higher mobility of $HCO^{\bullet}$ and $^{\bullet}CH_2OH$. Thus, these radicals could be stored within the ice mantle in cold regions and later react in warmer environments such as in star forming regions and comets. This is consistent with the gas phase detection of GA and EG in such environments (Hollis et al. 2000, 2001, 2002; Maury et al. 2014; Jørgensen et al. 2012; Beltrán et al. 2009; Coutens et al. 2015; Crovisier et al. 2004).* It has to be noted that the $HCO^{\bullet}$ and $^{\bullet}CH_2OH$ radicals can also efficiently formed from UV photolysis of ices rich in methanol (Öberg et al. 2009; Jacox & Milligan 1973) which may also contribute to GA and EG formation in star forming regions. All these arguments strengthen the fact that the mechanism (1) would be the dominate pathway for GA and EG formation in interstellar conditions.

Interestingly, GA and EG have been both detected toward the Sagittarius B2 north source known as the Large Molecule Heimat (LMH) with the same extended spatial scale (> 60") unlike GA isomers methylformate and acetic acid that are concentrated in a small spatial scale nearby the LMH source (<5") (Hollis et al. 2001, 2002).

These observations suggest that GA and EG formation (*i*) occurs in the same emitting volume, (*ii*) results from a common molecular filiation and (*iii*) does not necessarily need energetic processing such as UV photons to be formed, and (*iv*) the formation pathways of methylformate and acetic acid differ from the GA and EG one. This is consistent with our experimental results. In mechanism (1) (Fig. 7), only hydrogenation reactions and radical recombination are needed, which mainly proceed via barrierless or low barrier reactions. Moreover, GA and EG according to this mechanism are unavoidable by-products in the methanol formation from CO hydrogenation and thus they should be both detected in the same environment. In addition, it has been experimentally shown that the hydrogenation processing of CO ices at low temperature forms GA and EG but not methylformate (Fedoseev et al. 2015). This could be due to higher rate of $^{\bullet}CH_2OH$ radical formation compared to $CH_3O^{\bullet}$ from hydrogenation reaction of $H_2CO$ as shown in our experiments. Alternatively, methylformate may be formed trough grains surface reaction in ices rich in methanol triggered by UV photons (Öberg et al. 2009), which may explain the observation of methylformate in a small spatial scale nearby the LMH source. Additionally, we experimentally find a EG/GA ratio around 5 which is close to the values reported by Coutens et al. (2015) in comets where this ratio varies from 3 to 6 or in NGC 1333 IRAS2A class 0 protostar (EG/GA=5) in gas phase. However, it is really different from the one found in IRAS 16293-2422 class 0 protostar where this ratio is around 1 (Jørgensen et al. 2012). Several scenarios have been proposed to explain these differences. First the EG/GA ratio is similar in the grain mantles of low-mass protostars and it evolves either in solid phase by subsequent reactions of GA or EG, or in gas phase after their sublimation. In this case, if we assume that the EG/GA ratio will increase until it reaches the cometary value, it would mean that the changes in the gas phase ratio value can be due to difference in sublimation temperature between GA and EG or due to GA and/or EG destruction in the gas phase of the warm inner region by UV photon. In contrast, one can also think that the EG/GA ratio was already different in the grain mantle (Coutens et al. 2015) leading after desorption to different ratio values. The changes could be related to different grain mantle composition in protostars that may influence the GA and EG branching ratios. More experimental and theoretical works would have to be done to discriminate between these two scenarios.

## 6 CONCLUSION

In this work, using rare-gas matrix isolation techniques, we were able in a first time to form by VUV irradiation of formaldehyde formyl radical, $HCO^{\bullet}$. In a second time, after annealing of the photolysed Rg matrix, we form $^{\bullet}CH_2OH$ radicals from hydrogenation of $H_2CO$ within the Rg matrix. After sublimation of the Rg matrix, we observed the formation of glycolaldehyde (GA) and ethyleneglycol (EG) from the radical recombination, EG being the dominant species in our conditions with an EG/GA ratio of 5.1.

Based on our experiments, we propose a likely scenario

to explain the formation of GA and EG in the interstellar medium. First the needed radicals, namely $HCO^{\bullet}$ and $^{\bullet}CH_2OH$, are formed by successive hydrogenation of CO on the interstellar grain and then react to form EG and GA. This mechanism is entirely consistent with the detection of GA and EG in star forming regions and comets.

## ACKNOWLEDGEMENTS

This work has been founded by the French national program Physique Chimie du Milieu Interstellaire (PCMI), the Centre National des Etudes Spatiales (CNES), and the Provence-Alpes-Côte d'Azur region (PACA).

## REFERENCES

Ahlrichs, R., Bär, M., Häser, M., Horn, H., & Kölmel, C. 1989, Chemical Physics Letters, 162, 165
Alecu, I. M., Zheng, J., Zhao, Y., & Truhlar, D. G. 2010, J. Chem. Theory Comput., 6, 2872
Becke, A. D. 1993, J. Chem. Phys., 98, 5648
Beltrán, M. T., Codella, C., Viti, S., Neri, R., & Cesaroni, R. 2009, The Astrophysical Journal Letters, 690, L93
Bennett, C. J. & Kaiser, R. I. 2007, The Astrophysical Journal, 661, 899
Clark, J. H., Moore, C. B., & Nogar, N. S. 1978, J. Chem. Phys., 68, 1264
Cottin, H., Moore, M. H., & Bénilan, Y. 2003, The Astrophysical Journal, 590, 874
Coutens, A., Persson, M. V., Jørgensen, J. K., Wampfler, S. F., & Lykke, J. M. 2015, Astronomy & Astrophysics, 576, A5
Crovisier, J., Bockelée-Morvan, D., Biver, N., et al. 2004, Astronomy & Astrophysics, 418, L35
Deglmann, P., May, K., Furche, F., & Ahlrichs, R. 2004, Chemical Physics Letters, 384, 103
Diem, M. & Lee, E. K. 1979, Chemical Physics, 41, 373
Dubost, H. & Abouaf-Marguin, L. 1972, Chemical Physics Letters, 17, 269
Duvernay, F., Chiavassa, T., Borget, F., & Aycard, J.-P. 2004, Chemical Physics, 298, 241
Fedoseev, G., Cuppen, H., Ioppolo, S., Lamberts, T., & Linnartz, H. 2015, Monthly Notices of the Royal Astronomical Society, 448, 1288
Fuchs, G., Cuppen, H., Ioppolo, S., et al. 2009, Astronomy & Astrophysics, 505, 629
Hama, T. & Watanabe, N. 2013, Chemical reviews, 113, 8783
Hollis, J., Vogel, S., Snyder, L., Jewell, P., & Lovas, F. 2001, The Astrophysical Journal Letters, 554, L81
Hollis, J. M., Lovas, F. J., & Jewell, P. R. 2000, The Astrophysical Journal Letters, 540, L107
Hollis, J. M., Lovas, F. J., Jewell, P. R., & Coudert, L. 2002, The Astrophysical Journal Letters, 571, L59
Hudson, R. L., Moore, M. H., & Cook, A. M. 2005, Advances in Space Research, 36, 184
Jacox, M. E. 1981, Chemical Physics, 59, 213
Jacox, M. E. & Milligan, D. E. 1973, Journal of Molecular Spectroscopy, 47, 148
Jørgensen, J. K., Favre, C., Bisschop, S. E., et al. 2012, The Astrophysical Journal Letters, 757, L4
Keçeli, M., Shiozaki, T., Yagi, K., & Hirata, S. 2009, Molecular Physics, 107, 1283
Kerkhof, O., Schutte, W., & Ehrenfreund, P. 1999, Astronomy & Astrophysics, 346, 990
Khriachtchev, L., Tanskanen, H., Pettersson, M., et al. 2002, J. Chem. Phys., 116, 5708
Kunttu, H., Seetula, J., Räsänen, M., & Apkarian, V. 1992, J. Chem. Phys., 96, 5630
Maity, S., Kaiser, R. I., & Jones, B. M. 2015, Physical Chemistry Chemical Physics, 17, 3081
Maury, A., Belloche, A., André, P., et al. 2014, Astronomy & Astrophysics, 563, L2
Milligan, D. E. & Jacox, M. E. 1969, J. Chem. Phys., 51, 277
Nelander, B. 1980a, J. Chem. Phys., 73, 1026
Nelander, B. 1980b, J. Chem. Phys., 72, 77
Öberg, K. I., Garrod, R. T., Van Dishoeck, E. F., & Linnartz, H. 2009, Astronomy & Astrophysics, 504, 891
Pettersson, M., Khriachtchev, L., Jolkkonen, S., & Räsänen, M. 1999, The Journal of Physical Chemistry A, 103, 9154
Pettersson, M., Khriachtchev, L., Roozeman, R.-J., & Räsänen, M. 2000, Chemical Physics Letters, 323, 506
Pirim, C. & Krim, L. 2011, Phys. Chem. Chem. Phys., 13, 19454
Rimola, A., Taquet, V., Ugliengo, P., Balucani, N., & Ceccarelli, C. 2014, Astronomy & Astrophysics, 572, A70
Serrano-Andrés, L., Forsberg, N., Malmqvist, P., et al. 1998, J. Chem. Phys., 108
Sodeau, J. R. & Lee, E. K. 1978, Chemical Physics Letters, 57, 71
Treutler, O. & Ahlrichs, R. 1995, J. Chem. Phys., 102, 346
Verderame, F., Catellucci, E., & Califano, S. 1970, The Journal of Chemical Physics, 52, 719
Weigend, F. & Ahlrichs, R. 2005, Phys. Chem. Chem. Phys., 7, 3297
Werner, H., Bauer, C., Rosmus, P., et al. 1995, J. Chem. Phys., 102, 3593
Woods, P. M., Kelly, G., Viti, S., et al. 2012, The Astrophysical Journal, 750, 19
Woods, P. M., Slater, B., Raza, Z., et al. 2013, The Astrophysical Journal, 777, 90